Current Science
CS 6 (3), 6335-6344 (2026)
Received 25 March 2026 | **Accepted 24 April** 2026 | **Online Available 08 May** 2026
https://doi.org/10.52845/CS/2026-6-3-3

Current Science

Current Science

OPEN ACCESS

ISSN (O) 2795-8639

Original Article

Dynamic Analysis of Milling and Burr Morphology in 6061 Aluminum Alloy

Li Hongdan[1], Deng Shuang[1,2], Zhang Xinsheng[3]

[1]China Airborne Missile Academy, Luoyang 471009

[2]Nanjing University of Aeronautics and Astronautics, Nanjing 210016

[3]People's Liberation Army Unit 93160

***Corresponding Author: Li Hongdan**

Abstract:
6061 aluminum alloy is a common aluminum alloy material with good machinability and mechanical properties, which has been widely used in high-end manufacturing fields such as aerospace; Thin wall features are particularly common in the machining process of parts. This article uses a universal tool milling force mechanical model to model the dynamics of the machining process. Firstly, the cutting process is analyzed mechanically, and then the cutting force coefficient is identified through cutting experiments to obtain the milling dynamics model. The calculation results of the model are compared with the cutting experiment results, verifying the effectiveness of the model. The morphology of fine burrs in the machining process of parts was analyzed, and the relationship between machining parameters and burr morphology characteristics was experimentally studied, providing a certain reference for suppressing the formation of fine burrs in the machining of thin-walled aluminum alloy parts.

Keywords: aluminum alloy, dynamics model, milling, fine burrs, cutting test

1. Introduction

In recent years, China's aerospace industry and other high-end manufacturing rapid development, aerospace structural parts in order to achieve the goal of weight reduction design, a large number of 6061 aluminum alloy [1] was used. Such as factors the aviation structural parts are restricted by the factors such as narrow space and light weight of parts. The thin-wall structure is easy to be deformed, the rigidity of the parts is uneven, and it is easy to produce fine burrs have brought great difficulties to mechanical processing [2]. Aluminum alloy thin-walled parts are usually machined by the NC machining center. In the machining process, the cutting force, clamping force, cutting heat and other factors influence, the machining results are difficult to control accurately, and the resulting fine burrs easily cause the precision parts size out of tolerance [3].

In the numerical control machining process, the aluminum alloy thin-walled parts have poor rigidity, and it is easy to "let the knife" phenomenon. The actual track produced by the contact point between the tool and the part is quite different from the theoretical track, resulting in the inconsistency between the actual machining results and the program simulation results [4, 11-12]. In order to improve the qualified rate of thin-walled aluminum alloy parts and suppress the fine burrs, it is necessary to deeply study the machining process, establish the mathematical model analysis to quantitatively analyze the machining results [5, 15-16], and modify the

mathematical model through the machining test to explore the appropriate machining parameters and machining methods to effectively suppress the fine burrs in the machining process.

1. Dynamic Model Analysis

2.1 Cutting Force Model

For the flat-bottom milling tool, the accurate cutting force model is established to lay a foundation for the stability prediction of machining process. Therefore, in order to effectively analyze the cutting force, the cutting force model of dynamic cutting force due to the shear effect of chip formation on the rake face, the plough effect on the cutting edge and the plough effect on the back face is considered. In the modeling process, the resultant cutting force can be decomposed into axial, tangential and radial cutting force, and can be expressed as the product of cutting force coefficient, undeformed cutting thickness and cutting width.

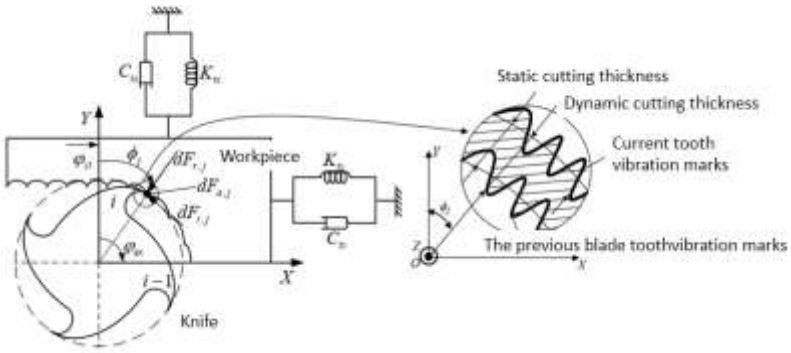

Figure 1: Vibration model for milling machining system

According to the mechanical model of cutting force of general-purpose tool proposed by Altintas, the milling tool is divided into n section beam elements with equal distance along the axial direction, then each section beam element has N cutter tooth pieces, then the j cutting tooth on the i section beam element is affected by tangential cutting force dFt,j(ϕ(z),z), radial cutting force dFr,j(ϕ(z),z)and axial cutting force dFa,j(ϕ(z),z), as shown in the vibration model of milling system, the corresponding cutting force can be expressed as

$$\begin{cases} dF_{t,j}\left(\phi(z),z\right)=K_{te}ds(z)+K_{tc}h_j\left(\phi_j(z)\right)db(z) \\ dF_{r,j}\left(\phi(z),z\right)=K_{re}ds(z)+K_{rc}h_j\left(\phi_j(z)\right)db(z) \\ dF_{a,j}\left(\phi(z),z\right)=K_{ae}ds(z)+K_{ac}h_j\left(\phi_j(z)\right)db(z) \end{cases} \quad (1)$$

Where:

Ktc,Krc,Kac-shear force coefficients of tangential, radial and axial directions;

Kte,Kre,Kae-edge cutting force coefficient of tangential, radial and axial force directions; h(ϕj,z)-the instantaneous undeformed chip thickness corresponding to the j th cutter tooth of the cutter tooth piece of the section i; fz-Feed per tooth of milling tool; ϕj(z)-the radial intrusion angle of the cutter tooth j at the axial cutting depth z, which varies with the change of the axial height z of the cutter;ϕ(z)-radial immersion angle of reference blade; ϕp-tool tooth angle; β-tool helix angle; D-diameter of cutting tool; db(z)-cutting width; ds(z)-length of cutting edge microelement. In formula (1),

$$\begin{cases} h_j\left(\phi_j(z)\right)=f_z\sin\phi_j(z) \\ \phi_j(z)=\phi(z)+j\phi_p-k_\beta z \\ \phi_p=2\pi/N \\ k_\beta=\left(2\tan\beta\right)/D \end{cases} \quad (2)$$

The cutting force obtained by Equation (1) is decomposed to the X, Y and Z axis directions,

and each cutting force expression under the tool coordinate system is obtained:

$$\begin{bmatrix} dF_{x,j}(\phi(z),z) \\ dF_{y,j}(\phi(z),z) \\ dF_{z,j}(\phi(z),z) \end{bmatrix} = \boldsymbol{T}_{i,j}(\phi_j(z),z) \begin{bmatrix} dF_{t,j}(\phi(z),z) \\ dF_{r,j}(\phi(z),z) \\ dF_{a,j}(\phi(z),z) \end{bmatrix} \quad (3)$$

In formula (3),

$$\boldsymbol{T}_{i,j}(\phi_j,z) = \begin{bmatrix} -\cos\phi_j(z) & -\sin\phi_j(z) & 0 \\ \sin\phi_j(z) & -\cos\phi_j(z) & 0 \\ 0 & 0 & 1 \end{bmatrix} \quad (4)$$

In combination with equations(1) and(3), the cutting force on the cutting edge of infinitesimal is integrated along the axial height of the tool, and the total cutting force received by the tool is obtained as follows:

$$F_q = \sum_{j=1}^{N} \int_{z_{j,1}(\phi_j(z))}^{z_{j,2}(\phi_j(z))} dF_{q,j}(\phi(z),z)dz, q = x,y,z \quad (5)$$

Where:

N-Number of Flutes on a Cutting Tool;

zj,1(ϕj(z))-The axial downward limit position of cutting tool; zj,2(ϕj(z))-The axial upper limit position of cutting tool.

Therefore, the total cutting force on the milling tool can be expressed as:

$$F(\phi) = \sqrt{F_x(\phi)^2 + F_y(\phi)^2 + F_z(\phi)^2} \quad (6)$$

2.2 Identification Model of Cutting Force Coefficient

In the universal cutting force model, the cutting force coefficient is closely related to the workpiece material, tool structure, friction coefficient between tool and workpiece surface and given cutting parameters [6, 13-14]. Therefore, determining the cutting force coefficient is the basis for modeling the cutting process and analyzing the cutting force. The cutting force coefficient needs to be obtained by parameter identification through machining test.

In order to establish the cutting force model accurately, this article adopts a fast cutting force coefficient calibration method for flat-bottom milling tools. Through the test, the average cutting force of the tool in each machining cycle is obtained by changing the feed of each tooth under certain cutting depth. In order to reduce the influence of tool runout on the test results, the total cutting force in each spindle rotation cycle is evenly distributed, and this method can calculate the average cutting force on each tooth [9, 19].

In order to facilitate the modeling of cutting force, according to the universal tool cutting force model [10, 17 and 18], the tool is divided into n section beam elements equidistant along the axial direction, and then N cutter teeth are divided on each section beam element, then the total material removal amount in each cutter tooth period is fixed when the j cutting teeth on the i section beam element are subjected to the tangential cutting force dFt,j(ϕ(z),z), radial cutting force dFr,j(ϕ(z),z) and axial cutting force dFa,j(ϕ(z),z) acting on a given tool geometry, so the average cutting force is independent of the helix angle, and it is integrated in one period, and then the average cutting force in each period can be obtained by dividing the integrationϕp result by the inter-tooth：

$$\bar{F}_q = \frac{1}{\phi_p} \int_{\varphi_{st}}^{\varphi_{ex}} F_q(\phi) d\phi, \ (q = x,y,z) \quad (7)$$

The slotted milling test is the simplest method for parameter identification, where the cut-in angle $\phi_{st}$and cut-out angle ϕ_{ex} are equal to 0 and π. The average cutting force in each tooth cycle can be expressed as:

$$\begin{cases} \bar{F}_x = -\dfrac{Na_p}{4}K_{rc}f_z - \dfrac{Na_p}{\pi}K_{re} \\ \bar{F}_y = \dfrac{Na_p}{4}K_{tc}f_z + \dfrac{Na_p}{\pi}K_{te} \\ \bar{F}_z = \dfrac{Na_p}{4}K_{ac}f_z - \dfrac{Na_p}{2}K_{ae} \end{cases} \quad (8)$$

From Equation (8) ,it can be seen that the average cutting force is a linear function of the feed per tooth, which can be expressed as:

$$\bar{F}_q = \bar{F}_{qc}f_z + \bar{F}_{qe}, (q = x, y, z) \quad (9)$$

Under the same cutting depth, a series of milling experiments were carried out, each time the feed parameters of each tooth were changed, and the average cutting force was treated by linear regression by measuring the average force of each tooth cycle. In this way, the feed force$\bar{F}_{qc}$and cutting force$\bar{F}_{qe}$under the corresponding cutting parameters can be calculated.

From equations (7) and (8),it can be seen that the cutting force coefficients in the cutting force model can be expressed as:

$$\begin{cases} K_{tc} = \dfrac{4\bar{F}_{yc}}{Na_p}, \quad K_{te} = \dfrac{\pi\bar{F}_{ye}}{Na_p} \\ K_{rc} = -\dfrac{4\bar{F}_{xc}}{Na_p}, \quad K_{re} = -\dfrac{\pi\bar{F}_{xe}}{Na_p} \\ K_{ac} = \dfrac{\pi\bar{F}_{zc}}{Na_p}, \quad K_{ae} = \dfrac{2\bar{F}_{ze}}{Na_p} \end{cases} \quad (10)$$

2.3 Identification Test of Cutting Force Coefficient

In order to simplify the identification process of cutting force coefficient, the whole machining test is conducted by means of groove milling. The test equipment adopts YHVT850Z CNC machining center, the tool adopts Carbide Endmill, the workpiece material is 6061 aluminum alloy, the cutting force acquisition sensor is Kistler9257B three-way force meter and corresponding data acquisition system. The tool geometry parameters and experimental scheme design are shown in Table 1 and Table 2 respectively.

Table 1.Cutter Parameters, Milling Methods And Milling Conditions

Tool material	Workpiece material	Tool diameter(Mm)	Blade length	Helix angle(°)	Pattern	Milling conditions
YG8	Aluminum alloy	0.5	4	35	Down milling	Dry milling

Table 2.Average Cutting Force At Different Feed Rates Per Tooth

Experiment Number	Spindle speed (rpm)	Axial Cutting depth（mm）	Feedrate per blade(mm/tooth)	$\bar{F}_x$ (N)	$\bar{F}_y$ (N)	$\bar{F}_z$ (N)
1	6000	0.4	0.02	-18.8309	12.8533	7.9037
2			0.04	-27.8604	15.2646	10.9034
3			0.08	-38.1705	16.1771	13.2204
4			0.1	-47.1842	15.9653	15.1172
5			0.12	-54.9654	16.1769	18.2453

The average cutting force for the different feed per tooth parameters in the test are shown in Table 2. The corresponding cutting force coefficients calculated by formulas (8) and (10) are as fallows:

$$\begin{cases} K_{tc} = 207.5\,N/mm^2, \quad K_{te} = 63.69\,N/mm \\ K_{rc} = 2080\,N/mm^2, \quad K_{re} = 47.6\,N/mm \\ K_{ac} = 390.7\,N/mm^2, K_{ae} = 20.397\,N/mm \end{cases} \quad (11)$$

2. Verification of Cutting Force Test

The cutting force coefficient and chip load can be determined by using the method of cutting force coefficient identification. By substituting these two parameters into the cutting force prediction model, the cutting force under different cutting conditions can be predicted and calculated. In order to verify the accuracy of the cutting force prediction model, a cutting test was carried out, and the measured cutting force data were compared with the predicted value [20].

The conditions of the equipment used in the milling test are the same as described above. In the test, the milling mode is thin-walled slotting. We set the rotation speed of the main shaft as 6000 rpm, the radial cutting width as 0.2 mm, the axial cutting depth as 0.4 mm, and the feed per tooth as 0.05 mm. The test results show that the theoretical predicted cutting force is basically consistent with the change trend of the test measurement results (as shown in Fig. 2). Only at cutting-in and cutting-out time, the measured cutting force fluctuates greatly, which may be caused by instantaneous cutting impact and chip breaking. These results prove the validity and accuracy of the cutting force prediction model.

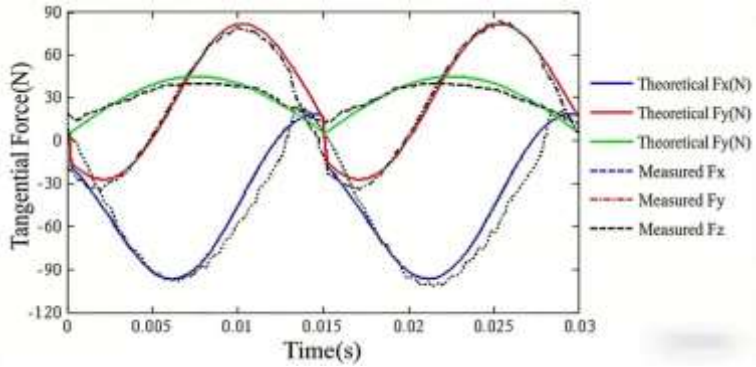

Figure 2:Comparison between predicted cutting force values and experimental measurement results

3. Analysis of Slot Milling Edge Defect Characteristics

4.1 Test on Slotted Milling of Simulated Parts

Due to the low hardness and soft material characteristics of aluminum alloy parts in milling, the burr suppression in micro-machining becomes a challenge research. Through conductinging micro-milling test without cutting fluid, the formation process and main forms of burrs were studied, and the influence of cutting factors on burrs under single-factor conditions and the influence under multi-factor coupling conditions were analyzed.

80×60×8 mm^3soft aluminum alloy 6061 test sample (Fig.3) shall be selected for the test. In order to eliminate the influence of original surface roughness on burr formation, the processing surface and four sides of the sample shall be finished before micro-milling test. Five 10 mm long milling grooves are machined at two sides of the length direction of the test sample with different process parameters (spindle rotation speed, feed speed and axial cutting depth), and then the cutting groove is machined at a distance of 5 mm from the end of the micro-groove through a macro-scale 4 mm diameter end milling cutter, so that the burr test milling groove does not penetrate the sample completely, and the burr at the end of the micro-groove is ensured to maintain the original morphology. The purpose is to divide the sample into small pieces, which is convenient for subsequent burr observation by SEM. The whole process is completed on the high-speed milling CNC machining center.

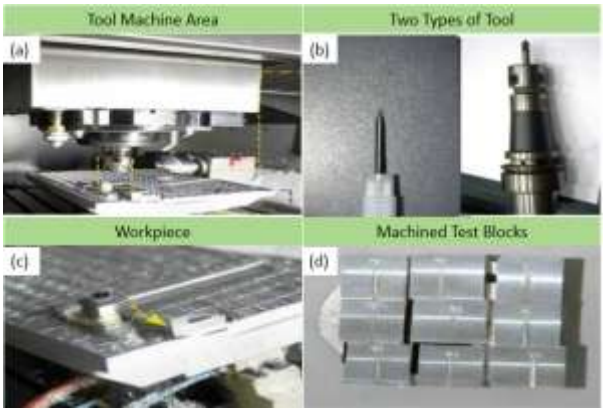

Figure3: Micro milling experimental setup and environment: (a) View of the machining area of the machine tool, (b) Groove milling cutter and cutting milling cutter, (c) Processed sample, (d) Processed experimental sample

Since the test focuses on the control of burr size and the influence of process parameters on the burr morphology to explore the burr formation mechanism, therefore, in order to avoid the high-speed scouring of cutting fluid on the burr formation, the test results are not significantly compared, and the cutting fluid is not added throughout the test process. According to BBD response surface method combined with CNC machining center performance, planning a three-factor and three-level experiment. Three different levels of spindle speed from 10000 r/min to 30000 r/m, three feed speeds from 100 mm/min to 300 mm/min, and three radial cutting depths from 0.05 mm to 0.15 mm were selected, there were a total of 17 experimental groups, as follows in Table 3. The axial cutting depth is 1 mm, and the milling groove axial direction is not penetrated through the sample, which is convenient for better fitting to the U-shaped groove processing working condition in the actual processing. Observe the burr shape at the outlet side of the U-shaped groove.

Table 3. Experimental Processing Parameters

No.	Speed(R/mm)	Feed speed (Mm/min)	Radial cutting depth(Mm)
1	20000	100	0.05
2	10000	300	0.1
3	30000	200	0.15
4	10000	200	0.15
5	30000	300	0.1
6	10000	100	0.1
7	20000	200	0.1
8	20000	100	0.15
9	20000	300	0.15
10	30000	100	0.1
11	20000	300	0.05
12	10000	200	0.05
13	20000	200	0.1
14	30000	200	0.05
15	20000	200	0.1
16	20000	200	0.1
17	20000	200	0.1

4.2 Analysis of Burr Forms

During processing, the form of burrs usually changes along with the variation of process

parameters. Compared with conventional machining, micro-milling cutter is more likely to wear during machining, and the radius of cutting edge is proportional to the thickness of undeformed chips. Since the processed sample materials in this study is 6061 aluminum alloy, its hardness is relatively low, compared with other materials, the bonding phenomenon is more obvious during processing, therefore, the inner curved burr accounts for a larger proportion of the burr size. Under the influence of high cutting temperature and cutting force, combined with the low hardness of micro-burrs of 6061 aluminum alloy, the formation of inner-bending burrs in machining is more obvious, which is mainly formed on the down milling side of groove. There are three types of internal curved burrs: Adhesive burrs, as shown in Fig.4 (a); Inward flowing burrs, as shown in Fig.4 (b);Clustered burrs, as shown in Fig.4 (c). The different forms of the above three burrs are mainly related to the feed speed in the process parameters. When the feed speed is maximum, the inner curved burrs are mostly in the form of adhesive burrs, which is because the larger feed speed can make the burrs on the side wall of the tool completely drawn into the groove after the feed of each tooth, so that the burrs are in the form of complete lamination. When the feed speed is the minimum, the inner bending burrs are mostly clustered, which is because too small feed speed will make the cutting edge multiple times of cutting or scraping the inner bending burrs that have been generated behind, so that it occurs secondary extrusion and folding; The flowing burr is a composite topography between the alove two points. Inwardly curved burrs hinder the direct visibility of the ground, and when the axial cutting depth is small, it is very easy to bond to the groove bottom surface, making it difficult to assess the surface condition.

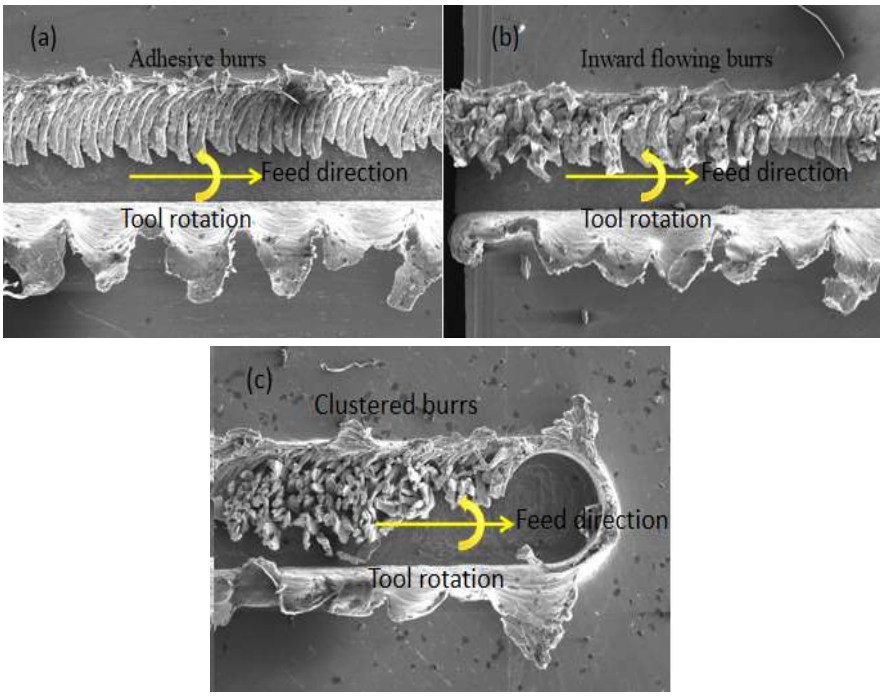

Figure 4:Typical morphological characteristics of inward and outward curved burrs

4.3 Effect of Process Parameters on Burr Size

FIG. 5 (a) shows the valgus burr width, inner curved burr width and the average burr width of the milled groove at the spindle speed of 10000 r/min, 20000 r/min and 30000 r/min respectively.

It can be seen from the data graph analysis that when the rotation speed and the feed speed are certain, the greater the axial milling depth, the greater the width of the valgus burr and the inner bending burr, in other words, the burr width is proportional to the axial cutting depth, This is because when the milling depth is large, the ploughing effect of the tool is significant, the maximum equivalent strain increases gradually, the cutting force also increases simultaneously, more metal chips need to be discharged from the milling groove, and thus the resulting burr width is larger. When the rotation speed and the axial milling depth

are certain, the larger the feed speed is, the larger the burr width is, that is, the feed speed is proportional to the burr width. This is because when the feed speed is large, the more obvious the cutting load phenomenon is, and at the high rotation speed, the more obvious the influence of the feed on the burr is, which is caused by the high wear rate of the processing material. Therefore, the formation of burrs can be reduced by using a smaller axial milling depth and a smaller feed speed at a low spindle speed.

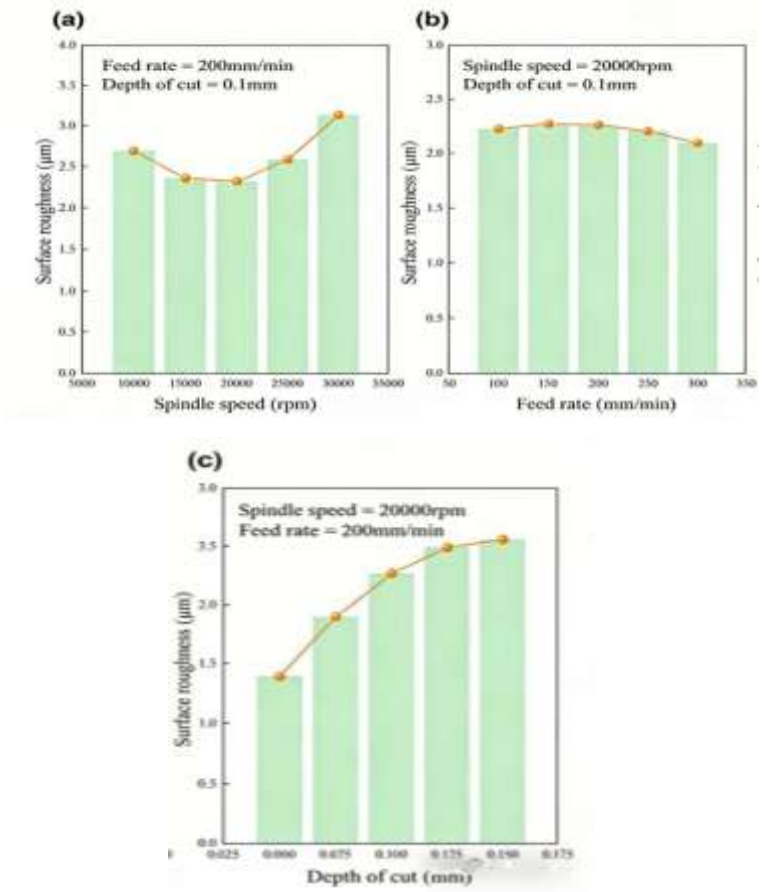

Figure 5: Data graph of maximum inner bending burr width, maximum outward turning burr width, and average burr width at different spindle speeds, feed rates, and axial milling depths

FIG.5 (b) shows the data of burr size at the feed speed of 100 mm/min, 200 mm/min and 300 mm/min respectively. When the feed speed and milling depth are fixed and the rotation speed is 20000 r/min, the size of burr is the smallest, and when the rotation speed is increased or decreased, the burr size is increased. This is because the cutting becomes slower at the low rotation speed and the tearing phenomenon is more obvious, while the cutting temperature is higher at the high rotation speed and the bonding phenomenon is more obvious because the material melting point is low, so the burr production amount is increased. As mentioned above, when the feed amount is high, a wide burr can be observed, but this phenomenon becomes inconspicuous at a high rotational speed. At high speed and cutting speed, the friction between the tool and the workpiece is reduced, and the chip flows through the surface of the tool under small resistance, so that the chip enters into the chip discharge groove and disengages, and the trend of milling burr formation is reduced. Therefore, it can be speculated that the formation of burrs can be effectively reduced by using high speed and high feed.

FIG.5(c) shows the schematic diagram of burr size under the milling depth of 0.05 mm, 0.1 mm

and 0.15 mm respectively. It can be clearly seen that the milling burr width shows the increasing trend from the left figure to the right figure. When the milling depth is 0.05 mm, the surface burrs are less, while when the milling depth is 0.1 mm and 0.15 mm, the surface burrs are obvious, and the width of the valgus burrs and the inner curved burrs on both sides of the milling groove increase.

By analyzing and comparing the test data, it can be concluded that the minimum average burr width is Test 1, Test 11 and Test 12 respectively, and the average burr width is less than 0.2 mm. After comprehensive evaluation of the three groups, it is not difficult to see that the milling depth of the three groups is the minimum 0.05 mm, while other parameters are different. This proves that the depth of milling is the most critical factor in the formation of micro-milling burrs, and the conclusion is consistent with that described above. When the average burr width changes, the maximum valgus burr width and the maximum inner bend burr width in the milling groove also change approximately the same trend.

4. Conclusions

Based on the cutting dynamic model of 6061 aluminum alloy and cutting test, the cutting force, burr shape and suppression method were studied.

(1) The milling dynamics model and parameter identification method are established for the thin-wall feature cutting process.

(2) Three-factor and three-level tests were carried out to deal with the problem that micro-burrs are easily produced in the machining of thin-walled aluminum alloy parts. The bonding phenomenon of 6061 aluminum alloy processing is obvious. The inner curved burrs account for a large proportion in the size of burrs, which can form adhesive burrs, inward flowing burrs and tufted burrs.

(3) The burr width is proportional to the axial cutting depth. The burr width decreases first and then increases with the increase of spindle speed, and increases first and then decreases with the increase of feed speed.

Acknowledgement

Funding The authors are grateful to the Aviation Science Fund (2023Z045012001).

References

1. Zhao Kai, Liu Zhanqiang, Wu Yuanchen.Study on Prediction of Milling Deformation of Aircraft Aluminum Alloy Thin Wall Parts [J].Tool Technology, 2014, 48(5).
2. Zhang Song, Li Binxun, Li Duohao.Progress in Finite Element Simulation of Cutting Process [J].Aviation Manufacturing Technology, 20 19, 62 (13): 14-28.
3. Ren Yuqiang, Li Guojian, Baihao.Research on Processing Technology of Large-scale Thin-wall Hard Aluminum Alloy Parts [J].Tool Technology, 2020, 54(4).
4. Liu Zhendong, Li Kaixun.Deformation Control of Aluminum Alloy Thin Wall Parts in Processing [J].China Technology Investment, 2017,000(023).: 284.
5. MA Junjin.Dynamic Modeling and Reconstruction Method of Magnetorh - eological Damping Support Fixture-Workpiece System [D].Northwest University of Technology.
6. Sun Yanyan, Cao Huibo, Li Yue.Experimental Study on Dimensional Precision of High Speed Milling of Aluminum Alloy Thin Wall Parts [J].Tool Technology, 2011,45(5).
7. Fu A J, Fu Y Q, Luo Z Y, et al.Experimental study on plastic instability of electromagnetic bulging for thin-walled aluminum alloy cylinder[J].Suxing Gongcheng Xuebao/ Journal of Plasticity Engineering, 2018, 25 (1):85-91.
8. Lee W S, Tang Z C.High Temperature Impact Deformation and Dislocation Substructure of 6061-T6 Aluminum Alloy[J].Journal of the Chinese Society of Mechanical Engineers,

Series C: Transactions of the Chinese Society of Mechanical Engineers, 2013(34-4).
9. Wang Chun, Su Bin, Tang Wuchu, et al..Numerical Simulation of High Speed Milling of 6005 A Aluminum Alloy [J]. Aviation Manufacturing Technology 2010 (15):77-81.
10. Gao Qiuge, Zhang Liqiang, Yang Jie, etc..Finite Element Analysis of Surface Residual Stress of Aluminum Alloy Based on ABAQUS Mirror Milling [J].Aviation Manufacturing Technology, 2024,67(6) :92-99.
11. Group forest, Ke Yinglin, Dong Huiyue.Study on Numerical Simulation of Cutting Force in Aviation Aluminum Alloy Milling [J].Acta Aeronautica, 2006,27(004) :724-727.
12. Shao Zidong, Sun Jie, Jia Xiujie, et al..Experimental Study on Cutting Force of Aluminum Alloy for High Speed Machining of End Milling Cutter [J].Combined Machine Tool and Automated Machining Technology, 2007(8):71-73.
13. Luo Heng, Wang Youqiang, Zhang Ping.Study on Surface Quality of 7A09 Aluminum Alloy Milling Based on Single Factor Method [J].Surface Technology, 2020, 49:327-333.
14. Tang Chaolan, Xie Yi.Multi-objective Optimization of 6061 Aluminum Alloy Milling Process Parameters [J].Journal of Guangdong University of Technology, 2020, 37(5).
15. Shen Wei, Li Bin.Study on Control of Surface Quality of Aluminum Alloy Parts by High Speed Milling Parameter Setting [J]. Engineering Technology Study, 2025(9).
16. Wang Xu, Li Zeyu.Research on deformation and control of special-shaped thin-walled aluminum alloy shell [J].China Equipment Engineering, 2025(8).
17. Lu Xiaohong, Luo Jiaqing, Cong Chen, etc..Prediction of burr size and process optimization of aluminum alloy LF21 micro-milling tip [J].Journal of Jilin University (Engineering Edition), 2025 (1)
18. Wang Yuchen, He Lihua, Rodney, etc..Effect of Process Parameters on Surface Quality of 7050 Aluminum Alloy Milling [J].Mechanical Science and Technology, 2024,43 :660-666.
19. Xu Yuanchang.Simulation Analysis and Experimental Study on Ultrasonic Vibration Assisted Milling of Aluminum Alloy Cutting Force [D].Qingdao University of Science and Technology, 2023.
20. Yu Bo, Zhang Zeyun, Song Jie.Typical NC Machining Scheme [J]. for Aluminum Alloy Sheet PartsMechanical Engineering and Automation, 2023(2):125-127.